Proc. Indian Acad. Sci. (Earth Planet. Sci.), Vol. 102, No. 3, September 1993, pp. 465–486.

Numerical simulation of upwelling off Visakhapatnam on east coast of India during pre-monsoon months

A D RAO, P C SINHA, S K DUBE and S CHAMARTHI
Center for Atmospheric Sciences, Indian Institute of Technology, New Delhi 110016, India

MS received 1 February 1993; revised 18 August 1993

Abstract. A three-dimensional numerical model of the type described by Johns and co-workers (1992), hereafter referred to as model (J), is applied to study the response of a coastal ocean to pure wind-stress forcing. Conservation equations are applied for mass, momentum, temperature, salinity and turbulence energy. Experiments are performed to investigate the evolution of the thermal structure and upwelling processes along the east coast of India during the pre-monsoon season. A comparison between the computed results and the limited observations on the thermal structure and alongshore currents over the inner-shelf off Visakhapatnam is presented.

Keywords. Bay of Bengal; numerical model; coastal upwelling; thermal structure.

1. Introduction

Over the Bay of Bengal two distinct wind systems prevail during the year – the summer or southwest monsoon and the winter or northeast monsoon winds. The wind-stress associated with these winds cause mass drift of oceanic waters leading to upwelling and downwelling along the east coast of India. Upwelling along the Visakhapatnam coast, a seasonal event occurring during the pre-monsoon period, is important for the local fishing industry. The annual variation of the thermal and salinity structure is documented by Rao *et al* (1986). Using direct current measurements during February to May of 1982, Rao and Rao (1989) have discussed alongshore currents over the inner-shelf off Visakhapatnam. However, there is no documentation reported by Rao *et al* (1986) and Rao and Rao (1989) on the dynamical structure of the coastal ocean. Consequently, it is worthwhile to consider a numerical model to study the dynamics, thermodynamics and salinity structure with suitable parameters. An appropriate model of the type developed by Johns *et al* (1992) has been used in the present investigation.

Using model (J), experiments were performed with different mean monthly wind-stress forcing representative of February to May. We analysed the evolving thermal and current structures in the coastal ocean off Visakhapatnam. The variability of the alongshore velocity field off Visakhapatnam and its influence on the upwelling during the pre-monsoon season has been examined. The computed thermal fields compare reasonably well with the observed fields documented by Rao *et al* (1986). The computed alongshore currents are also in qualitative agreement with the observations reported by Rao and Rao (1989).

2. Formulation of the model

The model used in the present study is based upon that described by Johns *et al* (1992). Accordingly, it is described briefly to focus on the basic formulation.

The origin, O, of a system of rectangular Cartesian coordinates is situated on the equilibrium level of sea-surface. Ox points towards east, Oy towards north and Oz is directed vertically upwards. The displaced position of the sea-surface is given by $z = \zeta(x, y, t)$ and the position of the sea-floor by $z = -h(x, y)$. A western coastal boundary is situated at $x = b_1(y)$ whilst there are open-sea boundaries at $x = b_2(y)$, $y = 0$ and $y = L$. The Reynolds averaged components of velocity (u, v, w) satisfy equations (Johns *et al* 1983, 1992).

$$\frac{\partial u}{\partial t} + u\frac{\partial u}{\partial x} + v\frac{\partial u}{\partial y} + w\frac{\partial u}{\partial z} - fv = -\frac{g}{\rho_0}\int_z^\zeta \frac{\partial \rho}{\partial x}\,dz - g\frac{\partial \zeta}{\partial x} + \frac{1}{\rho_0}\frac{\partial}{\partial z}(\tau_x), \tag{1}$$

$$\frac{\partial v}{\partial t} + u\frac{\partial v}{\partial x} + v\frac{\partial v}{\partial y} + w\frac{\partial v}{\partial z} + fu = -\frac{g}{\rho_0}\int_z^\zeta \frac{\partial \rho}{\partial y}\,dz - g\frac{\partial \zeta}{\partial y} + \frac{1}{\rho_0}\frac{\partial}{\partial z}(\tau_y), \tag{2}$$

In (1) and (2), f denotes the Coriolis parameter, ρ the local density of water and ρ_0 is a reference density. τ_x and τ_y denote components of Reynolds stress. The density is related to the local temperature and salinity by a linear equation of state given by

$$\rho = \rho_0(1 - \alpha T + \delta S). \tag{3}$$

where the constant α is a thermal expansion coefficient taken as 0·0002/°C and δ is the coefficient of salinity taken as $7{\cdot}5 \times 10^{-4}$/ppt.

Following Johns *et al* (1992), the dynamical boundary condition along the coastline leads to

$$u - vb_1'(y) = 0 \quad \text{at} \quad x = b_1(y), \tag{4}$$

whilst boundary conditions along the open-sea boundaries are

$$\bar{u} - \bar{v}b_2'(y) - \left(\frac{g}{h}\right)^{1/2}\zeta = 0 \quad \text{at} \quad x = b_2(y), \tag{5}$$

$$\bar{v} + \left(\frac{g}{h}\right)^{1/2}\zeta = 0 \quad \text{at} \quad y = 0, \tag{6}$$

$$\bar{v} - \left(\frac{g}{h}\right)^{1/2}\zeta = 0 \quad \text{at} \quad y = L. \tag{7}$$

In equations (5), (6) and (7), $\bar{u}, \bar{v}$ denote depth-averaged components of velocity defined by

$$(\bar{u}, \bar{v}) = \frac{1}{H}\int_{-h}^{\zeta} (u, v)\,dz \tag{8}$$

where H is the total depth, $\zeta + h$. As described in model (J), the wind-stress forcing is not applied adjacent to the alongshore open boundaries. Boundary conditions at

the impermeable sea-floor relate to absence of fluid slippage and they lead to

$$u = v = w = 0 \quad \text{at} \quad z = -h. \tag{9}$$

At the sea-surface, the internal Reynolds stress must be equal to the applied surface wind-stress $(\tau_x^\zeta, \tau_y^\zeta)$, so

$$\tau_x = \tau_x^\zeta \quad \text{and} \quad \tau_y = \tau_y^\zeta \quad \text{at} \quad z = \zeta. \tag{10}$$

Also, the surface kinematical condition requires that

$$\frac{\partial \zeta}{\partial t} + u\frac{\partial \zeta}{\partial x} + v\frac{\partial \zeta}{\partial y} - w = 0 \quad \text{at} \quad z = \zeta. \tag{11}$$

To accompany (1) and (2) the equation of continuity has the vertically integrated form

$$\frac{\partial \zeta}{\partial t} + \frac{\partial}{\partial x}(H\bar{u}) + \frac{\partial}{\partial y}(H\bar{v}) = 0. \tag{12}$$

Turbulence closure in the dynamical equations is achieved by making a gradient transfer hypothesis in which

$$\left.\begin{aligned} \tau_x &= K_M \rho \partial u/\partial z \\ \tau_x &= K_M \rho \partial v/\partial z \end{aligned}\right] \tag{13}$$

where the exchange coefficient, K_M, is finally related to the turbulent energy.

The temperature, T, and the salinity, S, satisfy an advection-diffusion equation of the form

$$\frac{\partial T}{\partial t} + u\frac{\partial T}{\partial x} + v\frac{\partial T}{\partial y} + w\frac{\partial T}{\partial z} = \frac{\partial}{\partial z}\left(K_T \frac{\partial T}{\partial z}\right) \tag{14}$$

and

$$\frac{\partial S}{\partial t} + u\frac{\partial S}{\partial x} + v\frac{\partial S}{\partial y} + w\frac{\partial S}{\partial z} = \frac{\partial}{\partial z}\left(K_S \frac{\partial S}{\partial z}\right), \tag{15}$$

where K_T and K_S are vertical diffusion coefficients for temperature and salinity, respectively. The boundary conditions to accompany (14) and (15) are

$$\partial T/\partial z = 0 \quad \text{at} \quad z = -h \quad \text{and} \quad z = \zeta, \tag{16}$$

$$\partial S/\partial z = 0 \quad \text{at} \quad z = -h \quad \text{and} \quad z = \zeta. \tag{17}$$

These conditions imply that there is no diffusive flux of thermal energy or salinity across the sea-floor and the sea-surface.

The coastal boundary is taken to be perfectly insulated with no heat transfer between the land and the sea. During the fluid outflow across the open-sea boundaries, the boundary temperature is determined by thermal advection from the interior of the relevant area. During fluid inflow, the boundary temperature is prescribed and in our application, it is kept constant according to its specified initial value just

outside the open-sea boundaries. Such a prescription is automatically incorporated in our choice of the finite-difference discretization of equations (14) and (15).

The parameterization of the turbulent processes is completed by the introduction of a transport equation for the turbulent energy density, E, and has the form

$$\frac{\partial E}{\partial t}+u\frac{\partial E}{\partial x}+v\frac{\partial E}{\partial y}+w\frac{\partial E}{\partial z}=K_M\left[\left(\frac{\partial u}{\partial z}\right)^2+\left(\frac{\partial v^2}{\partial z}\right)\right]$$
$$+\frac{g}{\rho_0}K_D\frac{\partial \rho}{\partial z}+\frac{\partial}{\partial z}\left(K_E\frac{\partial E}{\partial z}\right)-\varepsilon. \tag{18}$$

In (18), K_D and K_E are, respectively, diffusion coefficients for the vertical exchange of density and turbulence energy. On the right-hand-side of equation (18) the first term represents the production of turbulent energy by a vertical shear in the averaged flow. For $(\partial\rho/\partial z)<0$, the second term represents a sink of turbulent energy due to a stable density stratification. The third term represents vertical diffusion of turbulent energy with an eddy coefficient, K_E while the last term is the dissipation of turbulent energy.

Boundary conditions to accompany (18) state that there is no diffusive flux of turbulent energy across the sea-floor and the free-surface. We have

$$\partial E/\partial z=0 \quad \text{at} \quad z=-h \quad \text{and} \quad z=\zeta. \tag{19}$$

Following Li (1989), the representation of the exchange coefficients and the dissipation in terms of E is given by

$$\left.\begin{aligned} K_M &= c^{1/4}lE^{1/2}+N \\ K_T=K_S&=K_D=K_E=c^{1/4}lE^{1/2} \\ \varepsilon &= c^{3/4}E^{3/2}/l. \end{aligned}\right] \tag{20}$$

In (20), the value of the non-dimensional constant, c, is recommended by Launder and Spalding (1972) as 0·08. N is an externally prescribed mixing coefficient which reduces to negligible values both near the sea-surface and the sea-floor. The characteristic mid-depth value of N is $10^{-2}\,\mathrm{m^2\,s^{-1}}$. This type of vertical distribution is chosen to increase the vertical turbulent exchange of momentum in the mid-depths compared to salinity, thermal and turbulent energy. The detailed way in which the enhancement is incorporated into the model is described by Li (1989). It is sufficient to mention here that the incorporation is based upon the fact that the value of the vertical grid-spacing, Δz, is relatively coarser in the mid-depths compared with its values near the sea floor and sea surface. Utilizing this fact, the prescribed form used for N is made proportional to the local value of Δz. As a physical justification for the implementation of the procedure, a reference is made to work by Kundu (1984). In this, it is described how the vertical transfer of momentum is supported by both small scale turbulence and large scale internal gravity waves. Transfer by the latter is dominant in regions of strong stable thermal stratification where the shear production of small scale turbulence is suppressed. Since the internal gravity waves are not resolved in our model, their effect is parameterized by the vertical mixing enhancement procedure in regions where the turbulence energy, E, diminishes to negligible values. An alter-

native, and possibly a more physically-based method of proceeding may be to use the concept of stability functions as introduced by Mellor (1973). We must, however, emphasize that our scheme of closure based on the application of the turbulence equation is an essential ingredient for the success of the model when simulating processes that occur in the presence of a transient locally unstable thermal stratification. An application of an eddy viscosity model (even with the introduction of different stability functions for momentum and thermal energy processes) would require the parameterization of a scheme of convective adjustment in order to neutralize the effect of local unstable thermal stratification.

The length scale, l, is chosen to be consistent with a reduction in vertical mixing near the boundaries $z = -h$ and $z = \zeta$. Following Li (1989), it has an explicit form given by

$$l = \frac{k}{1/(z + h + z_{0b}) + 1/(\zeta - z + z_{0s})}, \tag{21}$$

where z_{0b} and z_{0s} are bottom and surface roughness lengths and k is von Karman's constant (0·4). In our application, we take $z_{0b} = z_{0s} = 0{\cdot}1$ cm. The results were found to be particularly insensitive to values of z_{0s} of this order and the principal role of the parameter is to prevent an occurrence of a zero in the mixing length scale at the sea surface. Nevertheless, during the monsoon season, a value of z_{0s} might be anticipated that is of order 1 m, this reflects the presence of high wave conditions. However, even with the application of such a value for the surface roughness, there is negligible effect on the response. The principal role of this z_{0s} is to prevent the occurrence of a mathematical singularity in the formulation. It should be observed that the relation (21) simulates only the gross features to be expected in the mixing length scale. A more refined representation (at the expense of further empiricism) might include a local reduction in the value of l in a thermocline region, although, with our present parameterization, there will still be an implied reduction in the value of K in a region of strong thermal stratification. It is because of this that the introduction of such a refinement does not lead to a significantly different type of response.

The solution of the model equations is described in detail in model (J). A system of transformed coordinates is introduced to incorporate the irregular coastal and bottom topography. The vertical coordinate is transformed to facilitate the implementation of boundary conditions at the sea-floor and the sea-surface. This leads to a new variable, σ, defined by $(z + h)/(\zeta + h)$. The transformed equations are then written in finite-difference form having a $20 \times 23 \times 36$ computational grid points along the east-west, the north-south and the vertical direction. The discretization scheme for (14) and (15) is identical to that utilized by Li (1989) and Johns *et al* (1992). It is based upon a scheme of upwind differencing described by Roache (1972). During fluid outflow, the upstream property of the scheme implies that the boundary temperature and salinity are being predicted from the analysis domain. During fluid inflow, the same property of the scheme results in a reference being made to the fluxes of temperature and salinity into the analysis domain. Our procedure is to specify these quantities on the basis of a temporally invariant temperature and salinity outside the analysis area. In the present context, these values are taken as the initial temperature and salinity. The inward advecting velocity, however, is calculated by extrapolation from the computed velocities in the interior of the analysis area. The

numerical solution of these equations is obtained by integration ahead in time with the prescribed wind-stress forcing given for a particular month of the pre-monsoon season.

3. Numerical experiments

Numerical experiments were performed by using the analysis area, bathymetry and the horizontal grid spacing analogous to that used in model (J). The analysis area is shown in figure 1 in which the origin, O, is within the equilibrium level of the sea-surface, it is situated at 79·9°E, 15·2°N. The Oy axis makes an angle of 53° with the north-south axis and is oriented in a generally north-easterly direction. The north-south extent of the area is approximately 800 km. We prescribe the wind-stress forcing in a limited analysis area which is analogous to that described in model (J). Accordingly, there is no wind forcing over a distance of approximately 145 km in the southernmost region of the analysis area. Similarly, there is a further unforced region which extends to a distance of 180 km in the northernmost part of the area (figure 1). The central part of the region in which the wind-stress forcing is applied extends over a distance of 475 km. The prescription of such unforced zones is found to be particularly effective in allowing the outward propagation of coastally trapped baro-

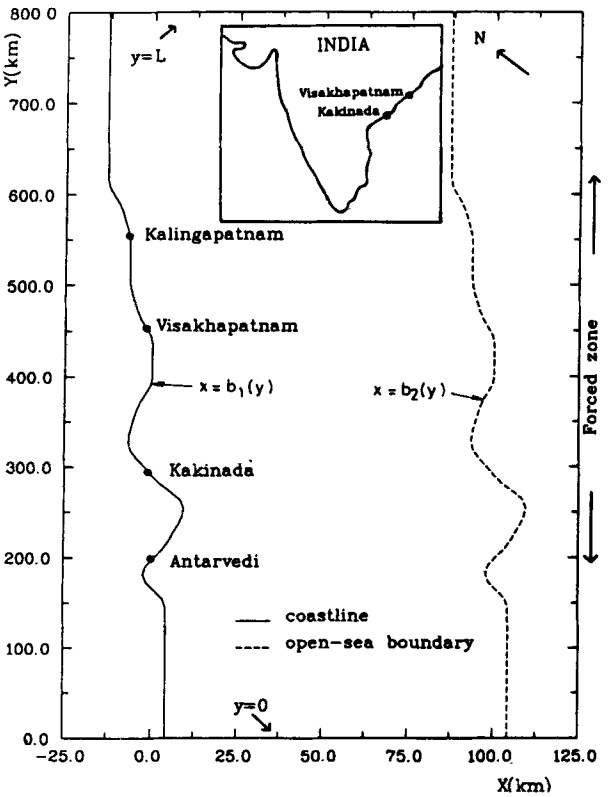

Figure 1. Plan of the analysis area. The inset shows the position of Visakhapatnam on the east coast of India.

tropic waves (Kelvin waves) across the alongshore open boundaries. The east-west extent of the area is uniform and equals 100 km. The geometry of the coastline modelled realistically between Antarvedi and Kalingapatnam each of which lies within the forced region. To the south and north of these positions, the actual coastline is replaced by a straight coastline pointing in the y-direction. As described in the finite-difference grid used in model (J) the first off-shore grid-point is about 1·7 km from the coastline and increases to about 6 km near the eastern open-sea boundary. Along y-direction, the implied grid-increment is about 36·5 km. Based on our experience, a fine grid-spacing is required both near the sea-floor and the sea-surface in order to resolve adequately the high shears that occur in these regions – especially that near $\sigma = 0$. It is, therefore, expedient to introduce a further transformation of the vertical coordinate to achieve this end. In our computations, the minimum depth at the coast is 10 m and maximum is 115 m in the deep region (near off-shore eastern open-boundary). Accordingly, the resolution at mid-depths is about 10 m in deep region whilst the resolution at the sea-bed is of the order of 1 cm. In the more shallow coastal upwelling zone, the resolution at the sea-bed is of the order of only 0·2 cm because the local depth is about 10 m. Thus, there is a full resolution of the important dynamical processes in the bottom Ekman layer.

The experiments are performed with the climatological mean monthly wind-stress forcings for the months of February-May from the winds (Hastenrath and Lamb 1979) by using a quadratic law. The value of the Coriolis parameter is taken as $5 \times 10^{-5}\,s^{-1}$ corresponding to the mean latitude of the Bay of Bengal.

All isotherms and isohalines in the model coastal ocean are horizontal before the onset of wind-stress forcing with a stratification representative of that applying to the Bay of Bengal in either February, March, April or May (Rao *et al* 1986). In all our experiments, we started the integration from an initial state of rest with the wind-stress forcing that corresponds to the different months of pre-monsoon period. Given that an upwelling event is essentially a transient phenomenon, it is difficult to select a time-level during the integration at which to compare computed and observed thermal fields. This problem is compounded by the fact that the observations in the cross shelf section will have been made at different times during the cruise period. Moreover, the quantitative detail in a predicted upwelling pattern will depend on the precise form of the initial conditions and the wind stress forcing. Bearing this in mind, we carried out an integration starting from the initial thermal field. The integration was continued for a period of 4 days. In a 4-day integration, upwarping of the isotherms is confined to 75% of the cross-shelf analysis zone. Additionally, the dynamical boundary condition applied along the eastern open boundary may possibly lead to a localized numerical contamination. Initial experiments, with an increased cross-shelf width of the analysis zone, showed that the results in the depicted coastal strip are completely uninfluenced by any such contamination resulting from an open boundary. It is also found that the propagation of coastally trapped waves would cause computational problems in longer integration beyond four days. The long period integration is only possible in the large-scale circulation models covering the entire Bay of Bengal. The model did not attain a steady state after 4 days, but the integration could not be extended for a longer period because of constraints on computer time.

The objective of these experiments is to show how the monthly evolution of the alongshore velocity field off Visakhapatnam affects upwelling during pre-monsoon

season. The results are restricted to the vertical cross-shelf section off Visakhapatnam. Observational data on the alongshore current varying with depth off Visakhapatnam coast are used for a comparison with the computed results.

In the first experiment, the model is integrated with the wind-stress forcing corresponding to the month of February (figure 2(a)). After 4 days of integration, figure 2(b) shows a plan view of the computed surface current vectors corresponding to the month of February. The entire flow field is predominantly westwards which is expected on the basis of the simple Ekman theory suggesting that the surface current is turned to the right of the direction of applied surface wind-stress.

The thermal structure in a vertical cross-shelf section off Visakhapatnam is shown in figure 3. The maximum sea-surface temperature is reduced to 27°C from its initial value of 27·3°C and the 27°C isotherm outcrops at the sea-surface. At depths less than 30 m, 24–26°C isotherms show a marked upwarping in a zone within 15 km off the coastline. Thus, the upwarping of the isotherms up to 30 m depth may be explained in terms of the upwelling induced by the local winds prevailing during the month of February.

The current vectors in a vertical cross-shelf section off Visakhapatnam are shown in figure 4. This may give a better understanding of the principal features in the computed dynamical fields off Visakhapatnam although there is no observational data on the current structure corresponding to the thermal field documented by Rao *et al* (1986). It is noticed that there is a weak onshore flow with maximum current

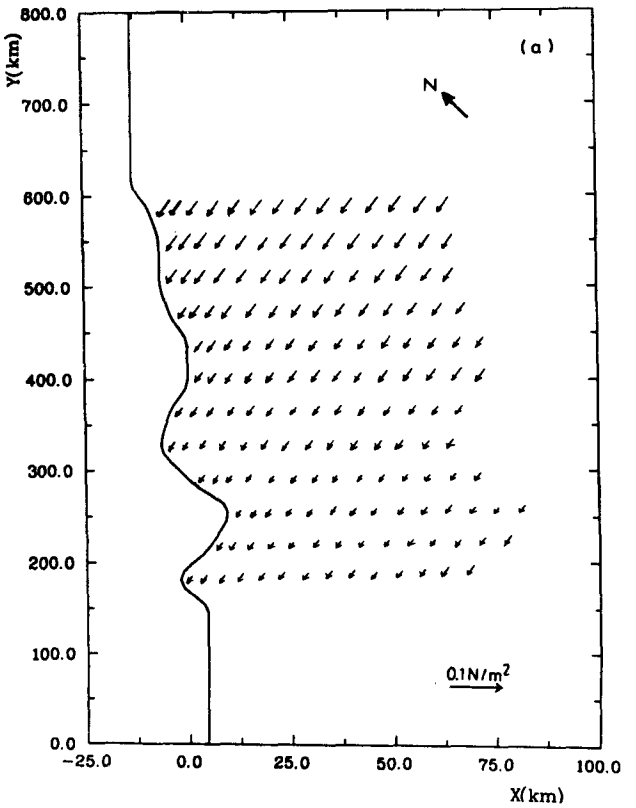

Figure 2(a). Wind-stress for February.

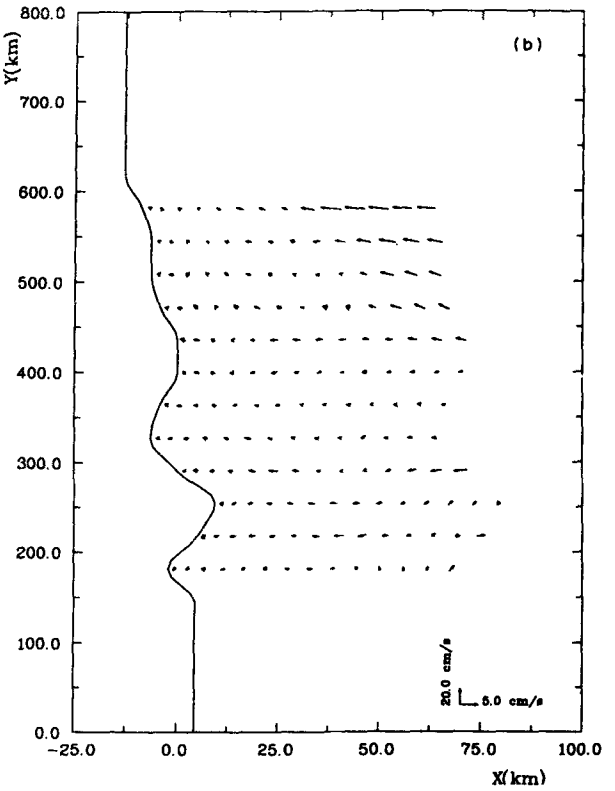

Figure 2(b). Plan view of the computed surface current vectors subjected to the February wind-stress forcing.

speeds of about 3·6 cms^{-1} at depths below 80 m. A weak offshore flow is observed in the sub-surface layers near the coastline which extends to a depth of 70 m with maximum current speeds of about 0·5 cms^{-1}. It is interesting to note the existence of weak upwelling with maximum velocities of about $2{\cdot}1 \times 10^{-3}$ cms^{-1} extending below 70 m depth. This fact demonstrates that the process of upwelling is just beginning in this month although the winds are not very favourable to this phenomena.

In the next experiment, the integration of the model is carried out with the wind-stress forcing for the month of March (figure 5(a)). Figure 5(b) gives a plan view of the computed surface current vectors corresponding to the month of March. Compared to the predominantly westward flow found for the month of February (figure 2(b)), it is beginning to turn slightly northwards. The strength of the flow is also observed to be increased in March when compared to February because the prevailing winds are stronger in March. The computed thermal field off Visakhapatnam is shown in figure 6. The upwarping of the isotherms are extended up to about 40 m depth compared to 30 m in the case of February. The temperature of near-coastal surface water has further reduced when compared to that for February. In figure 7, we have plotted the computed vertical current structure off Visakhapatnam. On comparing with figure 4 for the case of February, we notice that the upwelling velocity has increased from $2{\cdot}1 \times 10^{-3}$ cms^{-1} to $2{\cdot}9 \times 10^{-3}$ cms^{-1}. Although the direction of the flow is not clearly seen near the sea-bed, it is found that there is a very weak onshore

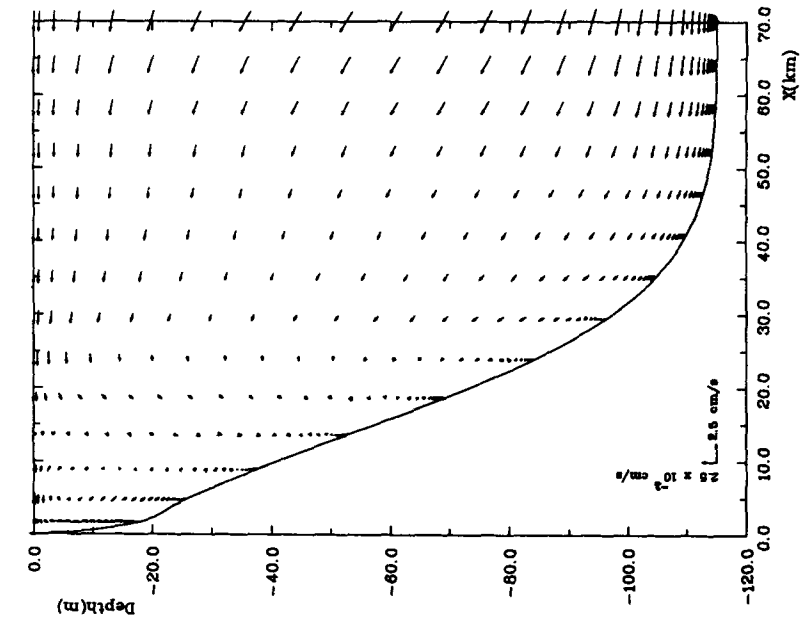

Figure 4. Computed current vectors in a vertical cross-shelf section off Visakhapatnam for the month of February.

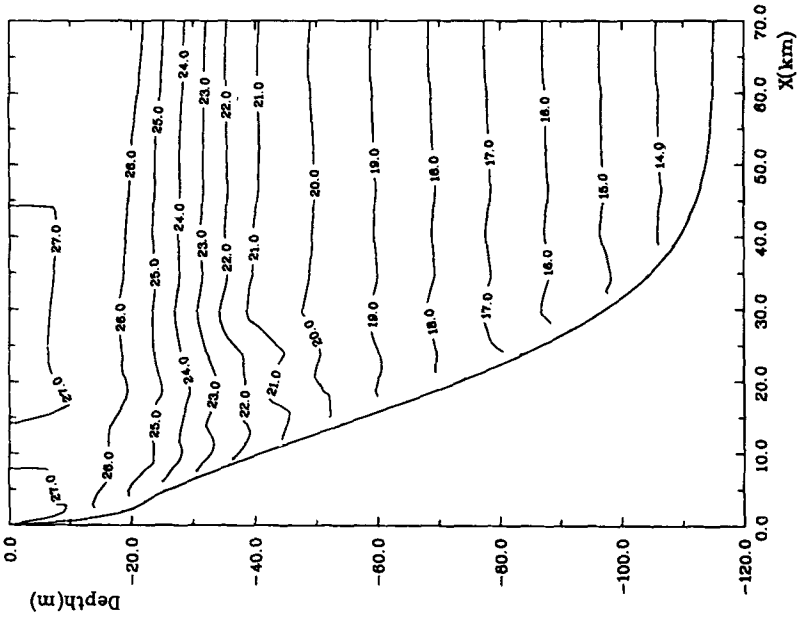

Figure 3. The computed thermal field off Visakhapatnam coast for the month of February. The numbers on the isotherms refer to temperature in °C.

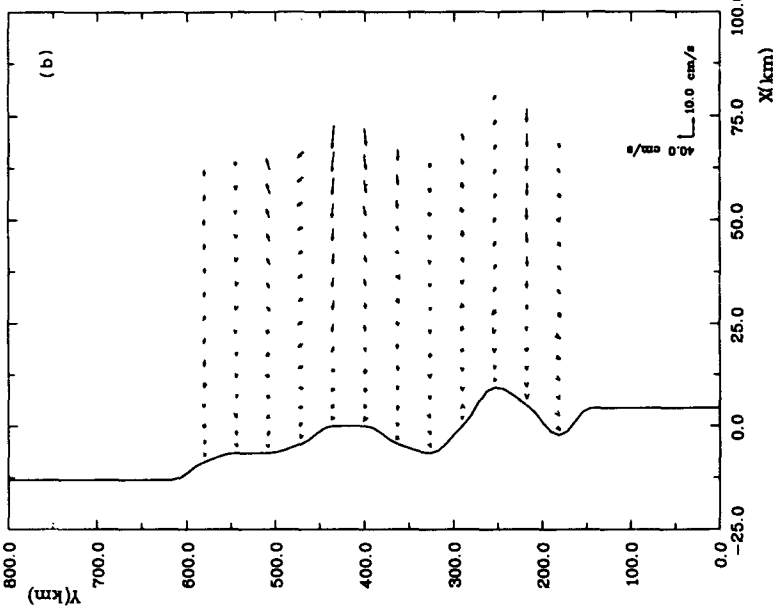

Figure 5(b). As in figure 2(b) except for the month of March.

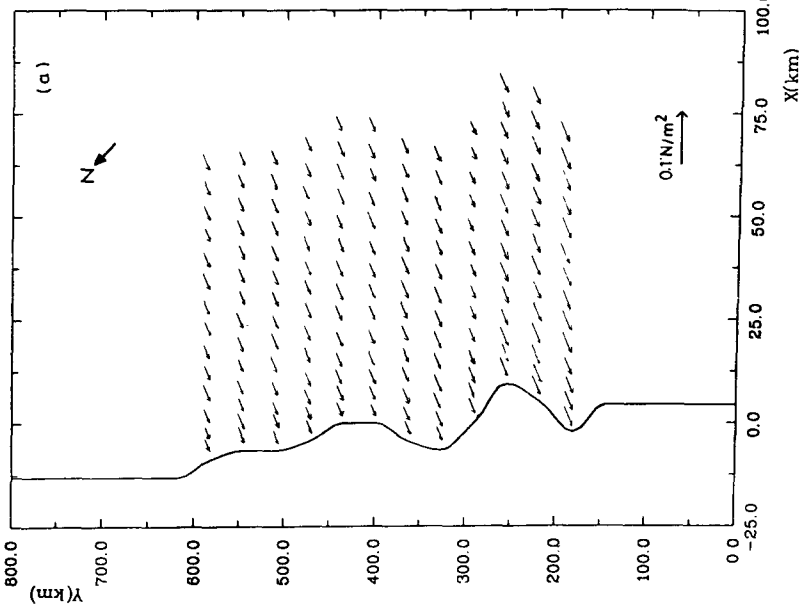

Figure 5(a). As in figure 2(a) except for the month of March.

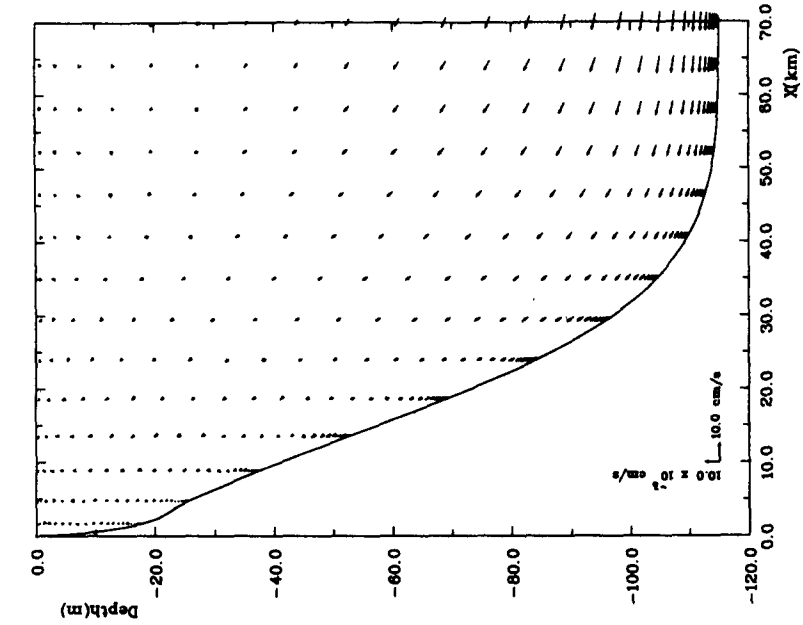

Figure 7. As in figure 4 except for the month of March.

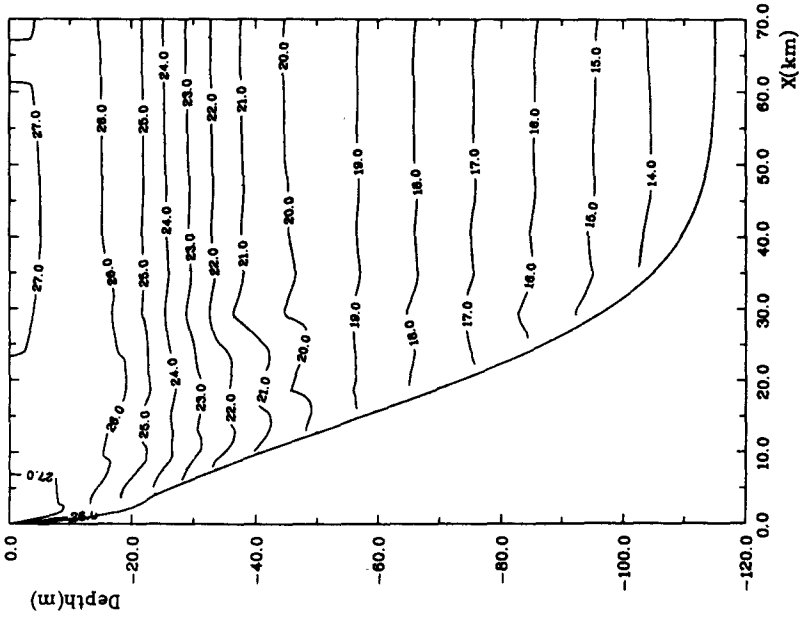

Figure 6. As in figure 3 except for the month of March.

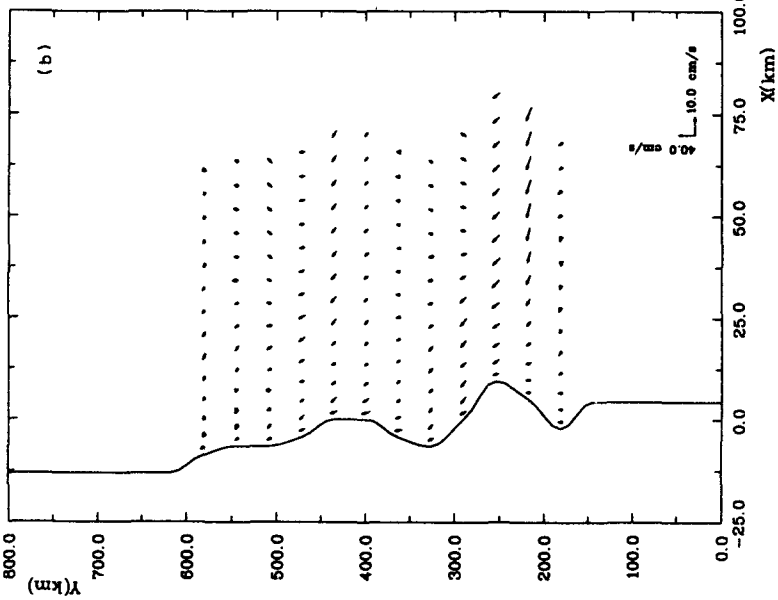

Figure 8(b). As in figure 2(b) except for the month of April.

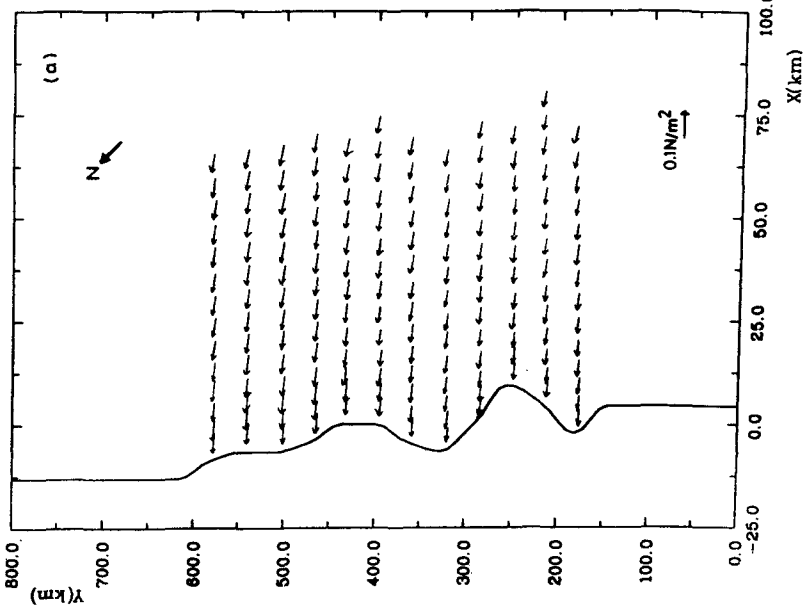

Figure 8(a). As in figure 2(a) except for the month of April.

flow extending from 10 m to deep waters. A weak off-shore flow is also noticed near the coast extending from surface to 10 m depth with a maximum value of 4 cms^{-1}.

The third set of experiment is carried out with the wind-stress forcing for the month of April (figure 8(a)). The computed surface currents corresponding to April are plotted in figure 8(b). The flow is now more north-westwards and the strength of the flow is further intensified compared to earlier months. The vertical thermal structure off Visakhapatnam for April is shown in figure 9. We notice that both 25°C and 26°C isotherms are intersecting the sea-surface indicating that the near-coastal surface water is cooled further. The sub-surface isotherms corresponding to 16–26°C all show a marked upwarping in a zone within about 15 km off the coastline and this feature is in clear contrast to those shown in figures 3 and 6. The vertical current structure off Visakhapatnam for the month of April is shown in figure 10. The only structural difference between figures 10 and 7 is the magnitude of the flow. The upwelling velocity has now reached a maximum of $3{\cdot}7 \times 10^{-3}$ cms^{-1}. The off-shore flow near the coast from surface to about 10 m depth is still weak with the maximum value similar to those for the month of March.

Finally, an experiment was performed with the wind-stress forcing for the month of May (figure 11(a)) which is known to be favourable for upwelling. A plan view of the computed surface current vectors are shown in figure 11(b). Away from the constraining influence to the coastline, the surface current is aligned towards a

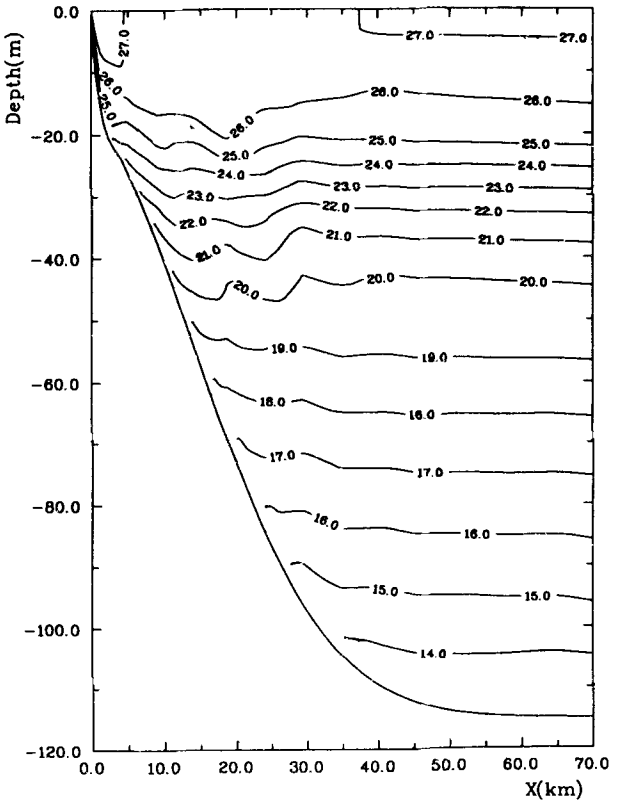

Figure 9. As in figure 3 except for the month of April.

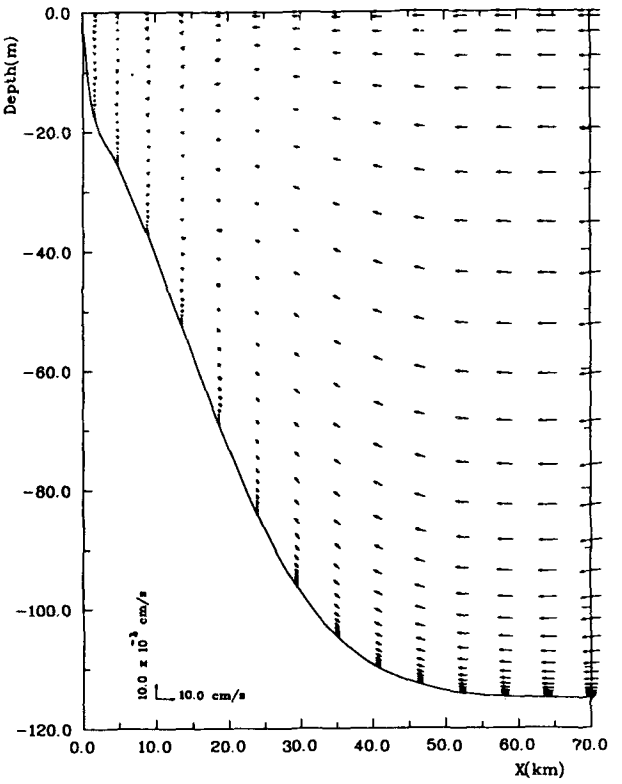

Figure 10. As in figure 4 except for the month of April.

northeasterly direction. However, in the vicinity of the coastline, the currents are parallel to the coast. The strength of the flow is more intense as the wind-stress forcing is larger compared to the previous months. The computed vertical thermal field off Visakhapatnam is shown in figure 12. The upwarping of the isotherms at all depths is evident from the figure. We also observed that there was a significant reduction of temperature at the sea-surface. It may be noted that the 27°C isotherm which outcrop at the sea-surface is further off-shore. The current vectors in a vertical cross-shelf section corresponding to the thermal field off Visakhapatnam is shown in figure 13. Although the surface flow direction is not clearly seen in figure 13, it is found that there is a weak off-shore directed flow in the surface layers with maximum speed of $1{\cdot}0\,\mathrm{cms}^{-1}$. The existence of onshore flow both in the bottom Ekman layer and within the interior of the ocean at depths below the sea-surface greater than 20 m may be seen. The unique feature of the present study is the predicted detail of the onshore flow at the bottom Ekman layer and is only produced because of a full resolution of near bottom processes. The onshore interior flow is geostrophically supported and is a product of an alongshore pressure gradient that develops because of the presence of alongshore inhomogeneities. Maximum onshore current speeds are about $11{\cdot}0\,\mathrm{cms}^{-1}$. The existence of strong upwelling is noticed in contrast to previous months throughout the flow field in the cross-shelf section. The computed maximum upwelling velocity is about $4{\cdot}0 \times 10^{-3}\,\mathrm{cms}^{-1}$.

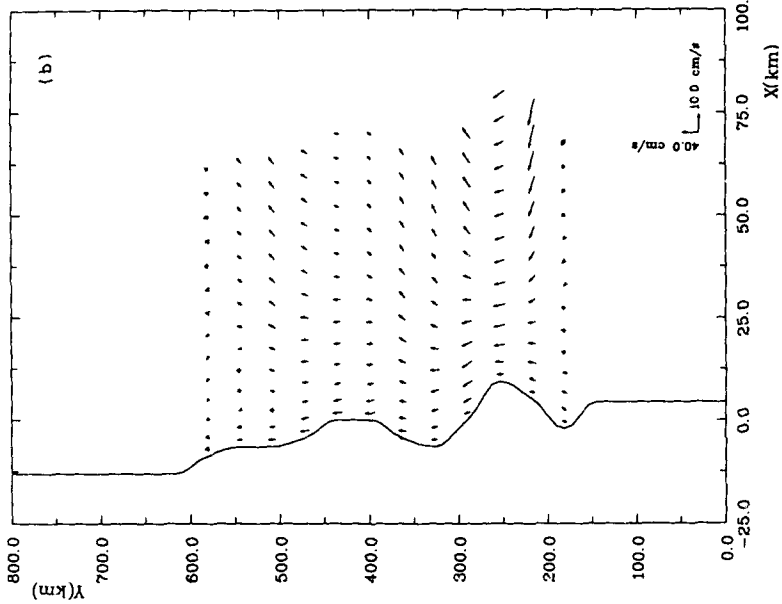

Figure 11(b). As in figure 2(b) except for the month of May.

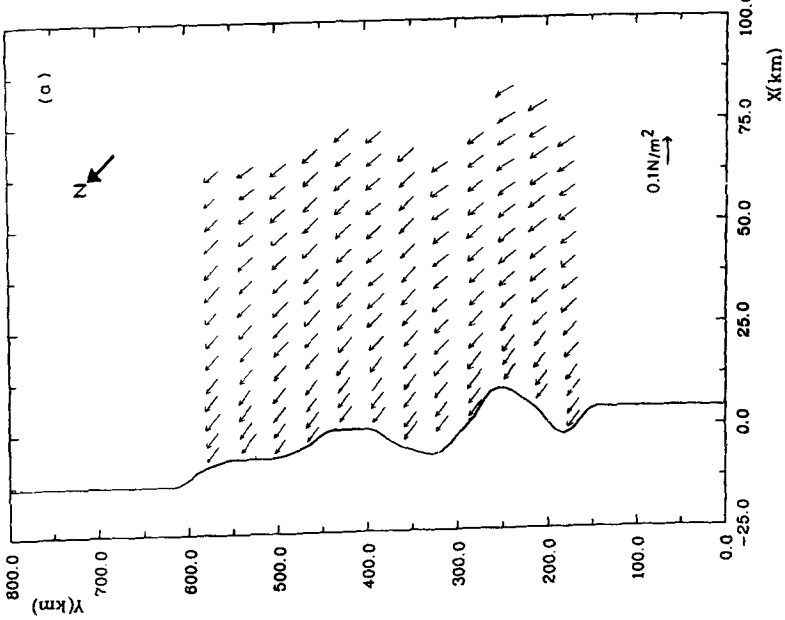

Figure 11(a). As in figure 2(a) except for the month of May.

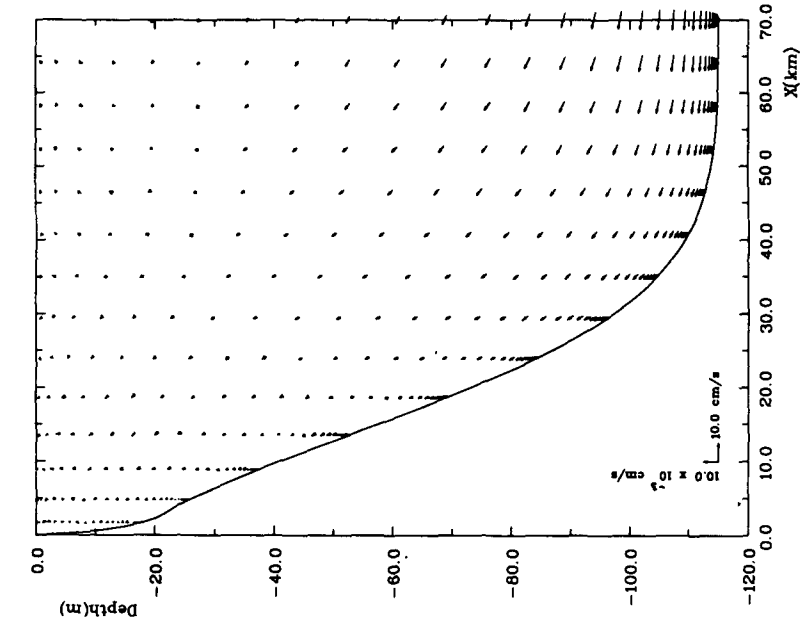

Figure 13. As in figure 4 except for the month of May.

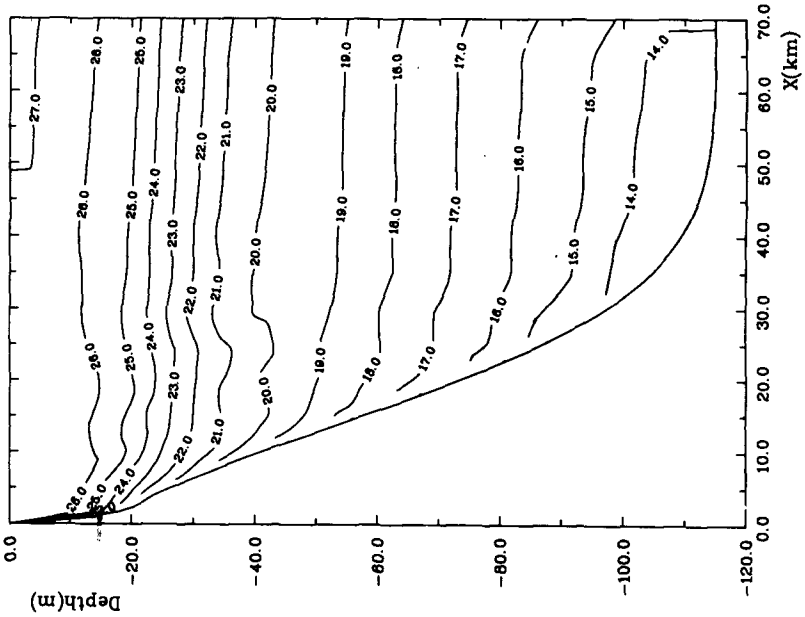

Figure 12. As in figure 3 except for the month of May.

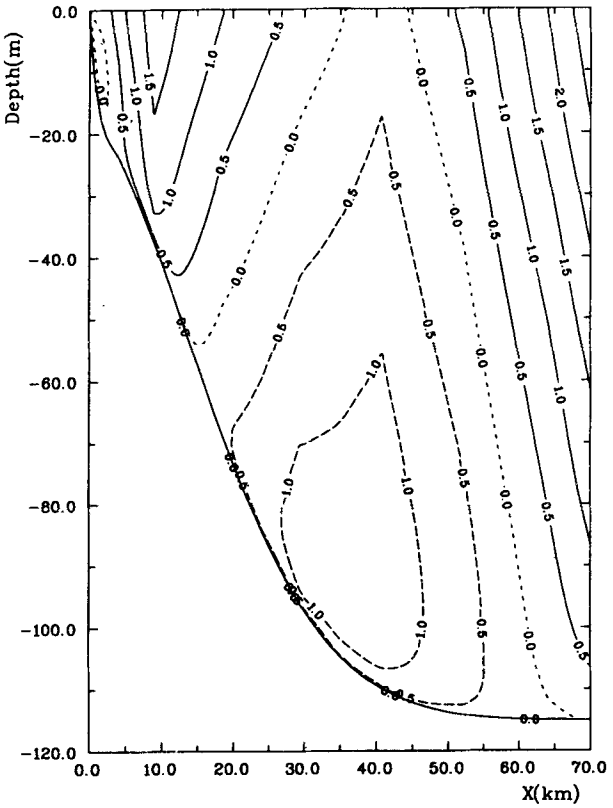

Figure 14. Isolines of the computed alongshore current in a vertical cross-shelf section off Visakhapatnam for February. The continuous lines refer to north-easterly directed currents. The broken lines refer to south-westerly directed currents. The numbers on the isolines refer to the current speed in cms^{-1}.

As limited data on the variability of alongshore velocity field off Visakhapatnam are available, it is worthwhile to analyse and compare the results of the respective months of pre-monsoon season with the observed fields. The discussions are limited only to alongshore component of the velocity which is responsible for upwelling during February – May. In figure 14, we delineate the same cross-shelf section off Visakhapatnam and show the isolines of the computed alongshore current structure due to the response of applied surface wind-stress for the month of February. A weak north-eastwards current is noticed in the near surface region adjacent to the coastline with a maximum speed of 1·5 cms^{-1}. A weak south-westward current, with a maximum speed of 1·0 cms^{-1} is observed at depths more than 50 m. A north-eastward current with a maximum speed of 2·5 cms^{-1} is again noticed all along the open eastern boundary. This oscillatory type of current structure in the vertical plane off Visakhapatnam is noticed only in the month of February. This feature may be attributed to the predominant westward wind-stress forcing in February associated with the eastern open-sea boundary condition. In figure 15, we show the alongshore current structure corresponding to March. Compared to figure 14, strong north-eastward current is noticed near the coast at the surface. Maximum current speeds of the order of 5·0 cms^{-1} are observed. Another notable difference is the absence of counter current

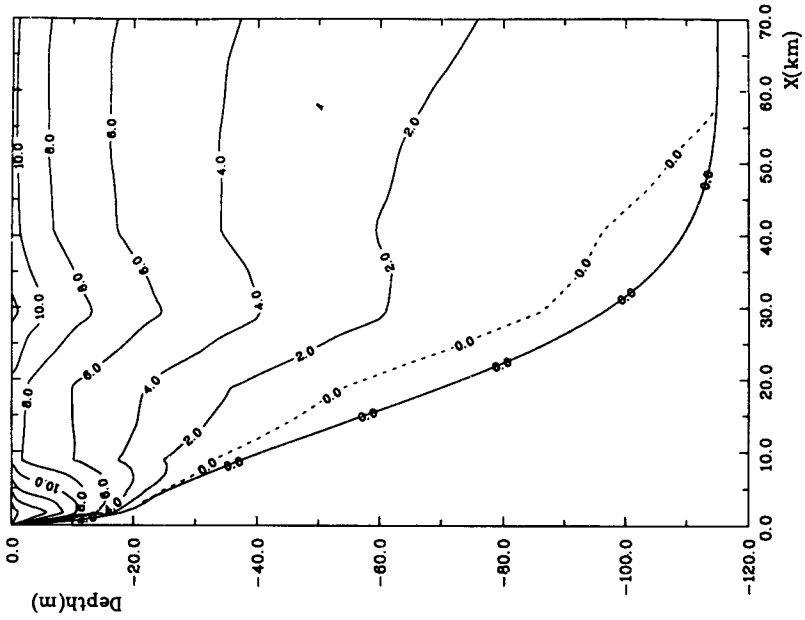

Figure 16. As in figure 14 except for the month of April.

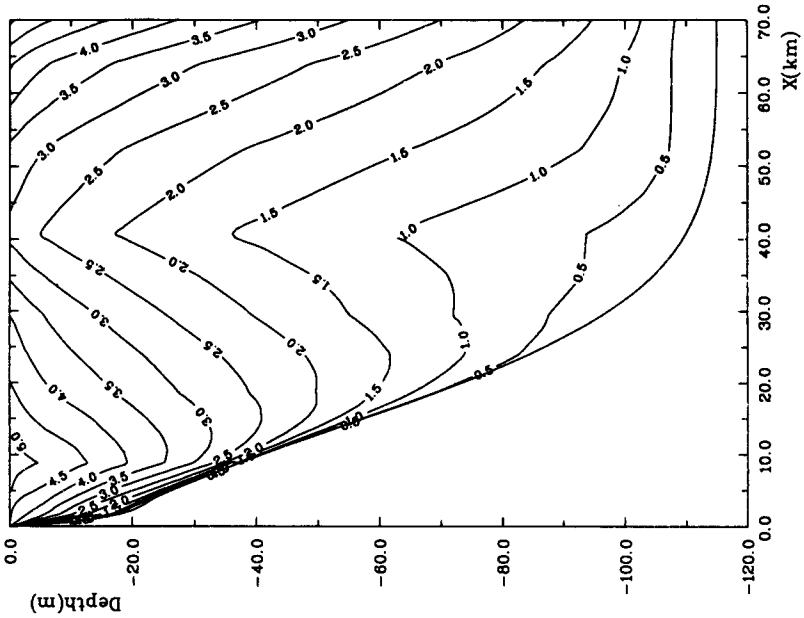

Figure 15. As in figure 14 except for the month of March.

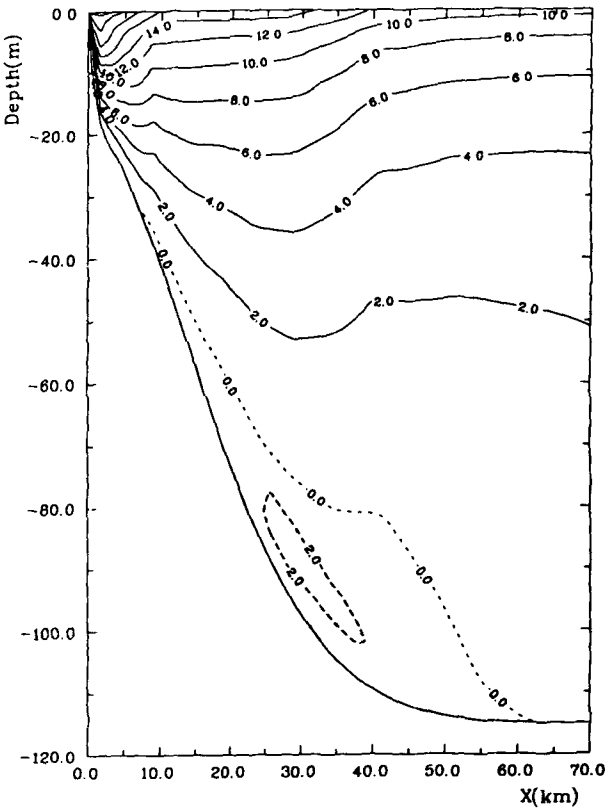

Figure 17. As in figure 14 except for the month of May.

at all depths in March. The isolines of the computed alongshore current for the month of April is given in figure 16. An intense core of alongshore currents in the near-surface region adjacent to the coastline is formed. The core extends to about 10 km from the coastline and up to a depth of about 15 m. Weaker alongshore currents of order 2 cms^{-1} are predicted at distances 70 km from the coast outside the intense core zone. The alongshore current structure for the month of May is shown in figure 17 in which we find that the direction of the flow is almost in agreement with the applied surface wind stress. The intensity of the alongshore currents in the core near the coast is further increased. The maximum speed of the north-east current is found to be 22 cms^{-1} and it extends to about 30 km from the coast. It is of interest to note that the formation of this baroclinic jet is supported quasi-geostrophically by the cross-shelf component of the pressure gradient resulting from the upwelled isotherms. At a depth below 80 m and a distance of 25 km from the coast there is a predicted weak counter current of maximum magnitude of 2 cms^{-1} flowing in the opposite direction to that of the surface currents. This is a consequence of the alongshore pressure gradient generated by alongshore inhomogeneities.

In figure 18, we reproduce the observed alongshore component of the monthly mean current over the inner-shelf off Visakhapatnam during the pre-monsoon period as documented by Rao and Rao (1989). We find that the surface and deep water currents are north-eastwards from February to April, while in May the flow changes

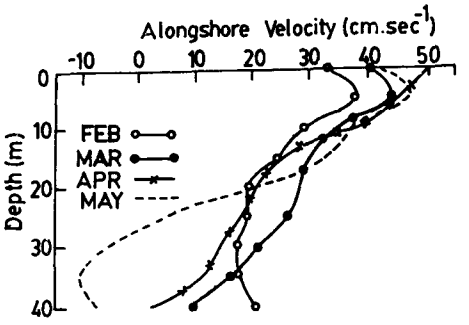

Figure 18. Observed monthly variation of alongshore currents over the inner-shelf off Visakhapatnam for February – May.

from northeast to southwest at a depth of about 27 m. A comparison with the corresponding computed fields depicted in figures 14–17 indicate an overall qualitative agreement. Although the magnitude of the maximum observed northeast currents for the month of February to May do not agree with the computed values, we find that the strength of the current in the simulation study increases from February to May. Another qualitative agreement between the observed and the computed currents relate to the changes in the flow direction during the month of May in the deeper layers of the coastal ocean. In the present paper, the computed vertical salinity structure off Visakhapatnam is not presented for discussions as there is no significant variation from one month to the other.

4. Conclusions

Numerical experiments were performed to simulate the thermal structure and the corresponding alongshore velocity field off Visakhapatnam for the pre-monsoon season. The observations made by Rao *et al* (1986) and Rao and Rao (1989) show a continued upwarping in the thermal structure and a steady growth in the magnitude of alongshore velocity from February to May. This is supported by the dynamic response on the basis of simple Ekman theory to the variation of local winds prevailing during this period. A comparison of the computed thermal structure and alongshore velocity field off Visakhapatnam with the observations of Rao *et al* (1986) and Rao and Rao (1989) provides support for the view that the coastal ocean is responding to the local surface wind-stress. Using a surface wind-pattern representative of that prevailing during February – May, we find that the dominant component of the alongshore surface flow is in the north-eastward direction with a maximum current magnitude of 22 cms^{-1} during the month of May. An interesting feature of the alongshore flow is the simulation of a deep counter current of order 2 cms^{-1} in the month of May. This is evidenced by the observations reported by Rao and Rao (1989).

The observational data of the coastal ocean off Visakhapatnam is inadequate and a network of data on various aspects is required for a full validation of the simulation study.

Acknowledgements

The authors are deeply indebted to Dr. B Johns, Department of Meteorology, University of Reading, U K for his critical reading of the manuscript and offering many helpful suggestions. A D Rao also acknowledges the financial support from the U K Overseas Development Administration to work at the University of Reading during 1990–91.

References

Hastenrath S and Lamb P J 1979 Climatic atlas of the Indian Ocean, Part-I: Surface climate and atmospheric circulation (Madison: University of Wisconsin Press), pp. 97

Johns B, Rao A D and Rao G S 1992 On the occurrence of upwelling along the east coast of India; *Estuarine, Coast. Shelf Sci.* **35** 75–90

Johns B, Sinha P C, Dube S K, Mohanty U C and Rao A D 1983 Simulation of storm surges using a three-dimensional numerical model: An application to the 1977 Andhra cyclone; *Q. J. R. Meteorol. Soc.* **109** 211–224

Kundu P K 1984 Numerical calculation of coastal flow with turbulent dynamics; *Deep-Sea Res.* **31** 39–60

Launder B E and Spalding D B 1972 Mathematical models of turbulence; (New York: Academic Press) pp. 169

Li Z 1989 A numerical study of basic coastal upwelling processes; Ph. D. Thesis, University of Reading, pp 283

Mellor G L 1973 Analytical prediction of the properties of stratified planetary surface layers; *J. Atmos. Sci.* **30** 1061–1069

Rao T V N and Rao B P 1989 Alongshore velocity field off Visakhapatnam, east coast of India during pre-monsoon season; *Indian J. Mar. Sci.* **18** 46–49

Rao T V N, Rao B P and Raju V S R 1986 Upwelling and sinking along the Visakhapatnam coast; *Indian J. Mar. Sci.* **15** 84–87

Roache P J 1972 Computational fluid dynamics (Albuquerque: Hermosa Publishers), NM pp. 434